Electric Power Systems Research 189 (2020) 106765

Contents lists available at ScienceDirect

Electric Power Systems Research

journal homepage: www.elsevier.com/locate/epsr

Classification and dynamic assessment of droop-based grid-forming control schemes: Application in HVDC systems

Ebrahim Rokrok*, Taoufik Qoria, Antoine Bruyere, Bruno Francois, Xavier Guillaud

L2EP, Univ. Lille, Arts et Metiers Institute of Technology, Centrale Lille, Yncrea Hauts-de-France, ULR 2697 - L2EP - Laboratoire d'Electrotechnique et d'Electronique de Puissance, F-59000 Lille, France

ARTICLE INFO

Keywords:
Droop control
Grid-forming control
HVDC systems
Inertia support
Power regulation

ABSTRACT

This paper introduces a novel classification for droop-based control strategies towards emerging interest of utilizing grid-forming control schemes in high voltage direct current (HVDC) systems. Classical droop control for grid-forming operation does not conventionally depend on a phase-locked loop (PLL). It is demonstrated that by including a PLL in droop control, it is possible to define two other droop-based control variants with different capabilities and functionalities. To highlight the differences in performance of each control scheme, the active power response of the power converter is evaluated in case of variation in grid short circuit ratio (SCR) as well as the PLL response time by considering an ideal DC bus. Accuracy in active power regulation, frequency support capability and virtual inertia emulation are the functionalities that have been addressed for the proposed three different control schemes. In a next step, the introduced droop-based grid-forming schemes are assessed by considering the dynamics of both AC and DC side of the power converter at one terminal of an HVDC link. Finally, based on the simulation results, a summary of features for all introduced grid-forming control schemes is presented[1].

1. Introduction

The massive integration of renewable energy resources (RESs) changes the generation paradigm from conventional fossil fuel-based power plants to renewable-based generation [1,2]. RESs are connected to the AC system through power electronic converters. Since power electronic converters do not inherently provide the inertial response to the power system, the increasing penetration of power electronic-based RESs is leading to a major reduction of the total electrical grid inertia and raising the rate-of-change-of-frequency (RoCoF) level in case of grid disturbances [3]. Such conditions are challenging in UK and Ireland due to the high penetration of wind power generation. In this case, the low inertia occurs when the load is low and high amount of power is imported from the existing and future high-voltage direct-current (HVDC) interconnections with the neighboring power systems [4].

Recent research projects have demonstrated that the control of HVDC converters with grid-forming control schemes, as fundamental to the operation of low-inertia power systems, could be an effective solution to increase the equivalent inertia and subsequently to improve the frequency dynamics of the power systems [5–7]. Therefore, several publications have focused on the implementation of virtual synchronous machines (VSMs), as one of the prominent grid-forming schemes, with an explicit emulation of the synchronous machine's (SM) swing equation on the HVDC converters [4,8,9].

There are several other grid-forming control schemes for virtual inertia emulation which have been reviewed in [10,11]. Many of these control schemes have nearly the same mechanism of operation. For instance, the classical droop control, which relies on the power-balance based synchronization mechanism, operates in a similar way to VSM. The application of the droop control in the control of the HVDC converters aiming to increase the power system's equivalent inertia is an emerging topic, which has not been much assessed. Only few number of publications have focused on the inertia emulation with the droop control in which the dynamics of the DC side of the converter have not been studied [12]. Conventionally, droop control does not depend on a phase-locked loop (PLL) for grid synchronization. Instability issue while connecting to the weak AC grids is a major concern related to including a PLL in the control system. This statement is originated from dynamic studies carried out on the grid-following control [13].

In this paper, three fundamentally different droop-based grid-

* Corresponding author.
E-mail address: ebrahim.rokrok@centralelille.fr (E. Rokrok).

[1] This work is supported by the project “HVDC Inertia Provision” (HVDC Pro), financed by the ENERGIX program of the Research Council of Norway (RCN) with project number 268053/E2, and the industry partners; Statnett, Statoil, RTE and ELIA.

https://doi.org/10.1016/j.epsr.2020.106765
Received 4 October 2019; Received in revised form 18 April 2020; Accepted 2 August 2020
Available online 08 August 2020
0378-7796/

forming control schemes with exclusive capabilities in power regulation accuracy, frequency support and inertial effect are proposed. These capabilities are examined by considering an ideal DC bus. The power electronic converter is assumed to be connected to a simplified equivalent AC grid where the interaction between the dynamics of the studied power converter with the remote grid is ignored. In order to investigate on the effect of including PLL in the grid-forming control, several simulations are performed by applying a step in the active power of the converter for various grid short-circuit ratios (SCRs) and PLL response times. The obtained and presented results, in both time-domain and state-space, highlight the fact that integrating the PLL in grid-forming control will not cause instability in case of connection to a weak AC grid, although the introduced grid-forming schemes have different dynamic performance with respect to the variation of the SCR and PLL response time. Analysis of the proposed control schemes, provides an additional insight into the application of the droop-based control variants in controlling an HVDC link. Therefore, in the last step by including the DC bus dynamics to the analysis, the introduced grid-forming schemes are examined in consideration of both DC and AC side requirements. Simulations, which are performed in Matlab-Simulink environment, show how the control of the DC side can be integrated with the droop-based grid-forming control schemes for HVDC applications.

The remaining of the paper is organized as follows. Section 2 recalls the fundamentals of the droop control for grid-forming controlled converters. Then, considering either with or without using a PLL, three different variants of the droop-based grid-forming control schemes are introduced and classified based on their capability in providing the virtual inertia for the power system. Section 3 addresses the dynamic assessment of the proposed control schemes in terms of variation in SCR and PLL response time and frequency support capability. The application of the proposed control schemes in control of the HVDC converters is discussed in Section 4. Finally, Section 5 concludes the paper.

2. Origin of grid-forming control for power converters

The grid-forming control has already been presented in many papers. Fundamental principles are now recalled to address the origin of this control and introduce its different variants. The studied power system consists of a DC/AC power converter, which is connected to an AC grid at the point of common coupling (PCC) by using a transformer (Fig. 1-a). The dynamics of the remote AC grid are ignored since the grid is modeled with a Thevenin equivalent circuit.

A grid-forming control is based on the phase and magnitude control of the output voltage v_f . To simplify the analysis, the filtering of harmonics is not considered. Therefore, v_f is assumed to be equal to v_m; the fundamental component of the modulated converter voltage. The effect of this assumption is discussed in Section 3.

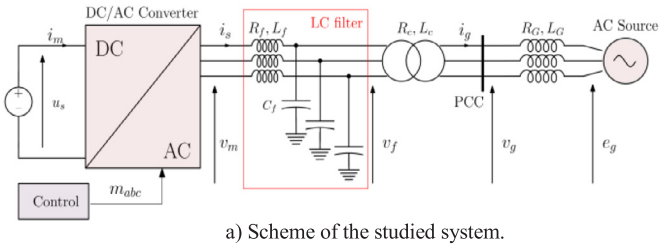

a) Scheme of the studied system.

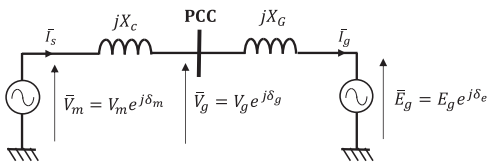

b) Simplified single-phase equivalent model of the system.

Fig. 1. Presentation of the studied system.

The simplified single-phase equivalent circuit of the system is given in Fig. 1-b. All the variables are considered in per unit. The transformer is only modeled by its leakage inductance X_c. It should be noted that upper case symbols stand for root mean square (RMS) values of instantaneous signals. Lower-case symbols represent the instantaneous signals. Based on this representation and by considering the voltage at the PCC (v_g), the active power can be expressed as [14]:

$$p = \frac{V_m . V_g}{X_c} \sin(\psi) \ (\psi = \delta_m - \delta_g), \tag{1}$$

where V_m and V_g are the RMS values for voltages and δ_m and δ_g are the corresponding phasor angles of the voltages in radian.

The active power is controlled through the difference of angle between the converter voltage angle δ_m and the grid angle δ_g. Let's consider that a PLL delivers an estimate of the phasor grid angle $\hat{\delta}_g$ at PCC. Then, it is possible to define a reference angle ψ_{ref} for the power control as follows:

$$\psi_{ref} = \delta_m - \hat{\delta}_g. \tag{2}$$

In steady state it yields:

$$\psi_{ref} = \psi. \tag{3}$$

Fig. 2 presents the grid-forming control using a PLL, which is named as scheme A. It should be noticed that since in transmission systems the angle ψ is small, then $\sin\psi \approx \psi$ [14]. In this figure, the phasor angles have been replaced by the time-domain angles. The expression of the instantaneous grid angle is:

$$\theta_g(t) = \omega_g \omega_B t + \delta_g, \tag{4}$$

where ω_B is the base frequency and ω_g the actual grid frequency. From Fig. 2, the converter angle θ_m is:

$$\theta_m(t) = \hat{\theta}_g(t) + \psi_{ref}(t), \tag{5}$$

with the sensed grid angle from a PLL:

$$\hat{\theta}_g(t) = \hat{\omega}_g \omega_B t + \hat{\delta}_g, \tag{6}$$

where $\hat{\omega}_g$ is the estimated grid frequency. In steady state $\hat{\omega}_g = \omega_g$ and $\hat{\delta}_g = \delta_g$. Eq. (5) can be written as $\psi_{ref}(t) = \theta_m(t) - \hat{\theta}_g(t)$ with $\hat{\theta}_g(t) = \omega_g \omega_B t + \delta_g$. Therefore, it can be found that by using the time-domain angles:

$$\psi(t) = \psi_{ref}(t). \tag{7}$$

In steady state ψ is constant and so, ψ_{ref} is constant. A closed loop control including an integrator is used to eliminate the power error in steady state (Fig. 2). Hence, in steady state, the measured active power is following the reference power p^*:

$$p = p^*. \tag{8}$$

Generally, a low-pass filter is applied to the power measurement. The aims are to filter the measurement noise, to avoid frequency jump and to decouple the dynamic of droop control loop from inner loops. Here, the filter is applied to the mismatch of the reference power and

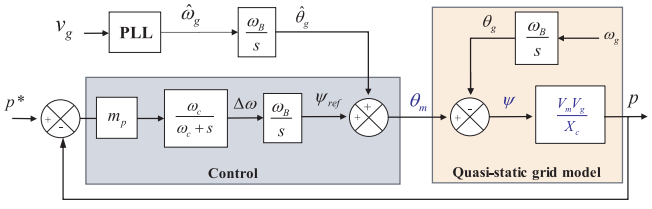

Fig. 2. Grid-forming control with a PLL - scheme A.

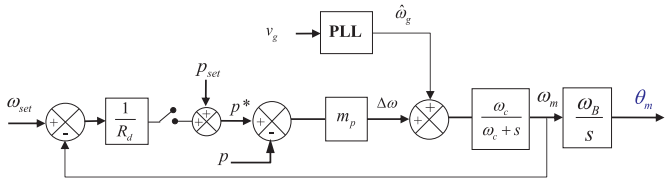

Fig. 3. Grid-forming control with a PLL - scheme B.

the measured power that provides the same effect [15]. The cut-off frequency of the filter ω_c has to fulfill the following condition to ensure the stable operation of power converter [16]:

$$\frac{\omega_{gn}.\ \omega_B}{20} < \omega_c < \frac{\omega_{gn}.\ \omega_B}{5}, \tag{9}$$

where ω_{gn} is the grid nominal frequency. Usually, $\omega_c = \frac{\omega_{gn}.\omega_B}{10}$ is chosen in the literature [15]. In [17] it has been demonstrated that the scheme A is highly robust against the variation of the grid short circuit ratio. Moreover, due to the desirable estimation of the grid angle, this grid-forming scheme can regulate the active power accurately. In Fig. 3, the information from the PLL has been moved to obtain another variant of the grid-forming schemes. The estimate of the grid angle is not used anymore but only the estimate of the grid frequency. The active power is still under control but not with the same dynamics.

For this control scheme, the differential equation that relates the angular frequency ω_m to the active power can be written as follows:

$$\frac{1}{m_p\omega_c}\frac{d\omega_m(t)}{dt} = p^*(t) - p(t) - \frac{1}{m_p}(-\hat{\omega}_g(t) + \omega_m(t)). \tag{10}$$

Eq. (10) is equivalent to the well-known swing equation in synchronous machines, which is recalled in Fig. 4. By identification, the equivalent inertia constant and damping factor are found as follow:

$$H = \frac{1}{2m_p\omega_c},\ K = \frac{1}{m_p}. \tag{11}$$

Therefore, the control scheme B is capable of providing an inertial effect, which is one of the main interests of using grid-forming control for future power systems. In steady state, $\omega_m = \omega_g$ and $\hat{\omega}_g = \omega_g$. It results in:

$$p^*(t) = p(t). \tag{12}$$

If the estimated frequency by the PLL is replaced by the nominal grid frequency ω_{gn}, (Fig. 5) a classical droop control is obtained and named, in this paper, as scheme C. In [17], it has been shown that:

$$\omega_g(t) - \omega_{gn} = m_p(p^*(t) - p(t)). \tag{13}$$

This last formula is equivalent to the classical inversed frequency droop control with the frequency droop gain m_p.If this converter is operating in parallel with other sources, it is well known that a good load sharing when supporting the frequency is linked with the choice of this droop gain. For example, the ENTSOE grid code for the generator prescribes a range of droop values between 1.5% and 10% [18]. Conversely, with the PLL (schemes A and B), m_p is a gain, which can be adjusted with respect to the desired closed loop dynamics and there is no link with the frequency support. Droop control can be implemented in an outer loop as illustrated in Fig. 3.

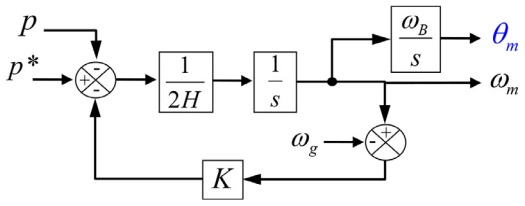

Fig. 4. Implementation of the swing equation.

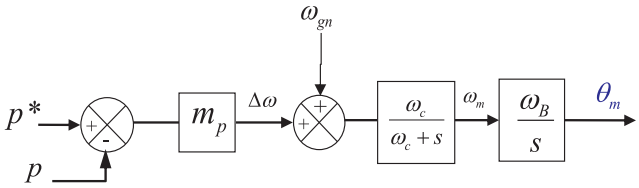

Fig. 5. Grid-forming control with no PLL - scheme C.

The corresponding differential equation of the scheme C is expressed by:

$$\frac{1}{m_p\omega_c}\frac{d\omega_m(t)}{dt} = p^*(t) - p(t) - \frac{1}{m_p}(-\omega_{gn} + \omega_m(t)). \tag{14}$$

As the result, this control scheme has the same inertial effect as the scheme B. The difference is that the value of m_p is not adjustable in the scheme C and it is determined based on the load sharing requirements. Therefore, ω_c is the only adjustable parameter to get the desired value of inertia constant.

To sum up, the three types of control have fundamentally different characteristics. Schema A provides only an active power control. Scheme B adds an inertial effect. Scheme C merge, three functionalities: active power control, inertial effect and frequency support. Although the scheme C has all abovementioned functionalities, in terms of frequency support, there is no possibility to limit the amount power that participates in the frequency support. This may be a big issue for the sources that are connected to this kind of converter.

3. Dynamic assessment of the grid-forming control variants

The aim of this study is to investigate on the robustness of the introduced droop-based grid-forming control variants as well as the frequency support capacities. To this end, the average model of the 2-level voltage source converter (illustrated in Fig. 1a) is used. It should be noted that in this stage, since the aim is to study only the AC side, an ideal DC source is considered. Dynamic simulations are performed in Matlab-Simulink environment. Control schemes are implemented in a synchronous reference frame (SRF) by using the Park's transformation [19].

The scheme of the dynamic model implementation is presented in Fig. 6. In [15, 20], it has been proved that the fast dynamics of inner control loops (voltage and current control) have a negligible effect on the system dominant poles. Therefore, all the pole map analysis are performed for the simplified model with no LC filter. Identical results in time domain for both simplified model and detailed dynamic model proves the correctness of the simplification assumption. Two following studies in grid-connected mode assess the functionalities of the three introduced grid-forming controls.

3.1. Connection to a constant frequency grid

In this case study, it is assumed that the power converter is connected to a constant frequency grid. A focus is made on the active power control. The dynamic response of the converter is assessed with respect to the SCR and PLL response time variations. System parameters are given in Table 1.

3.1.1. Variation of the SCR

According to IEEE definition, SCR is the ratio of the available short-circuit current, to the load current at a particular location [21]. At the PCC, SCR is expressed as:

$$SCR = \frac{1}{X_G} \tag{15}$$

Ref. [22] has defined the grid strength as strong, weak or very weak

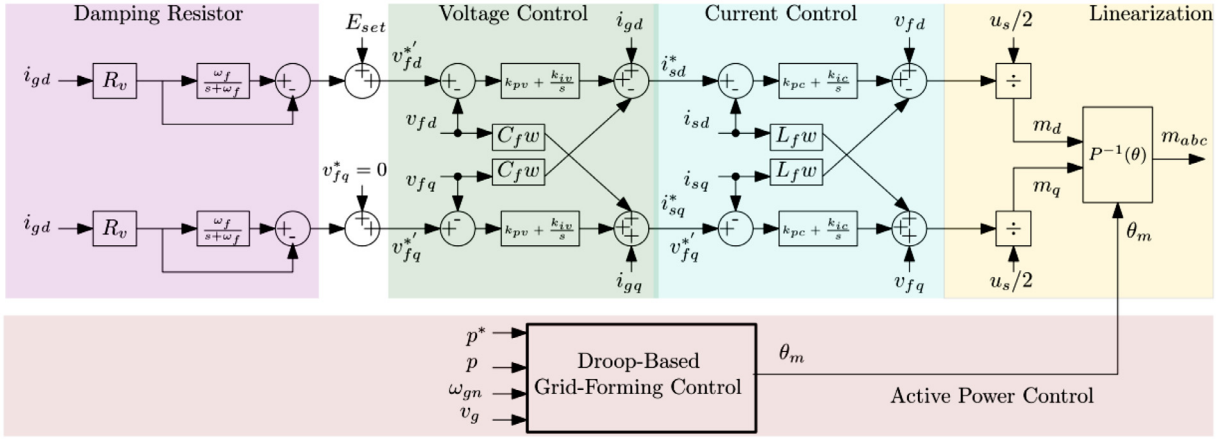

Fig. 6. Dynamic implementation of the grid-forming control [15].

Table 1
System parameters of Fig. 1.

Parameter	Value	Parameter	Value
Base power S_B	1 GW	p^*_{pu}	0.0 pu
Converter nominal power p_n	1 GW	m_p	0.02
Base voltage V_B	320 kV	ω_c	31.4 rad/s
Grid voltage E_g	1 pu	R_v	0.09 pu
Base frequency ω_B in rad/s	314.16	ω_f	60 rad/s
Grid nominal frequency ω_{gn}	1 pu	E_{set}	1 pu
AC line-line voltage	320 kV	L_f	0.15 pu
Transformer inductance X_c	0.15 pu	C_f	0.066 pu
Transformer resistance R_c	0.005 pu	k_{pv}	0.52
Grid Thevenin inductance X_G	0.333 pu	k_{iv}	1.16
Grid Thevenin resistance $R_G = X_G/10$	0.0333 pu	k_{pc}	0.73
u_s	640 kV	k_{ic}	1.19

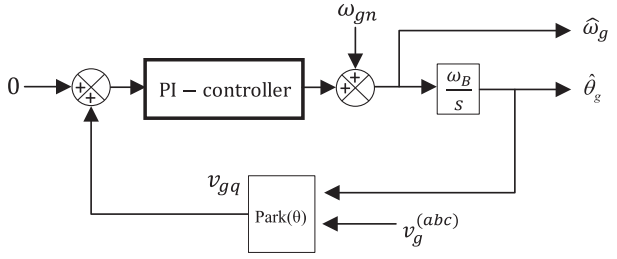

Fig. 7. Structure of the PLL.

if its SCR is greater than 3, between 2 and 3, or lower than 2, respectively. The given grid impedance in the Table 1 corresponds to the SCR = 3. The droop gain m_p is 2% for the scheme C. In order to have the similar dynamic behavior in active power control loop for SCR = 3, the adjustable parameter $m_p = 0.0062$ is considered for the scheme A (see Ref. [17]). The same value of m_p as scheme A is chosen for the scheme B. A PLL with 20 ms response time is used to provide an estimate of the grid angle and frequency at the PCC for schemes A and B. The basic block diagram of the PLL is illustrated in Fig. 7. Fig. 8 indicates the pole trajectory of the studied system for all control schemes with respect to the SCR. It can be clearly seen that, contrary to the scheme A, the system dominant poles are moving with respect to the SCR value for both schemes B and C. The theoretical origin of this statement has already been explained for scheme A and C in [17].

In the time domain, a step is applied to the power reference at $t = 0.2$ s. Time domain simulation with the full dynamic model of the system verifies the higher dependency of the active power dynamics for the schemes B and C to the value of SCR as it is illustrated in Fig. 9. Presented results show that the control scheme A is not sensible to the SCR and so it is very appropriate for the active power regulation. More significantly, while connecting to a weak grid by the PLL-based grid-forming schemes (schemes A and B), the system is not facing instability and it keeps an acceptable damping.

3.1.2. Variation of the PLL response time

In this case, the SCR is kept constant (SCR = 3) and the PLL response time is changing. Fig. 10 shows the pole trajectory of the studied

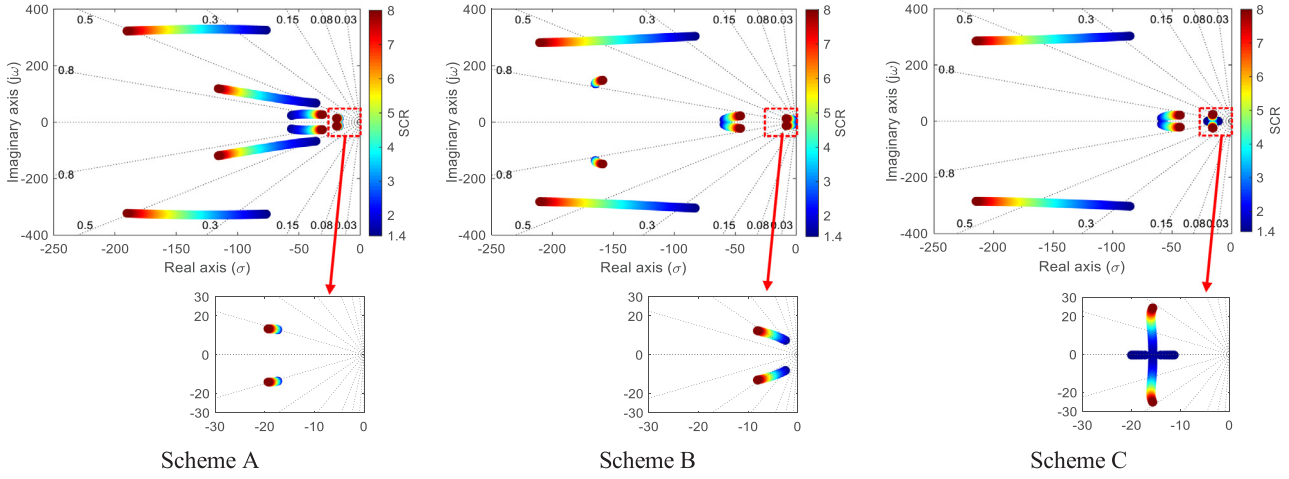

Fig. 8. System pole trajectory with respect to the SCR for each control scheme.

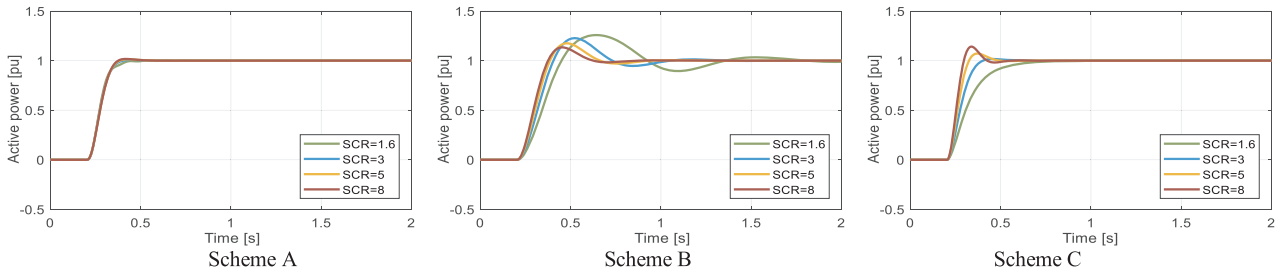

Fig. 9. Active power response of each control scheme with respect to the SCR variation.

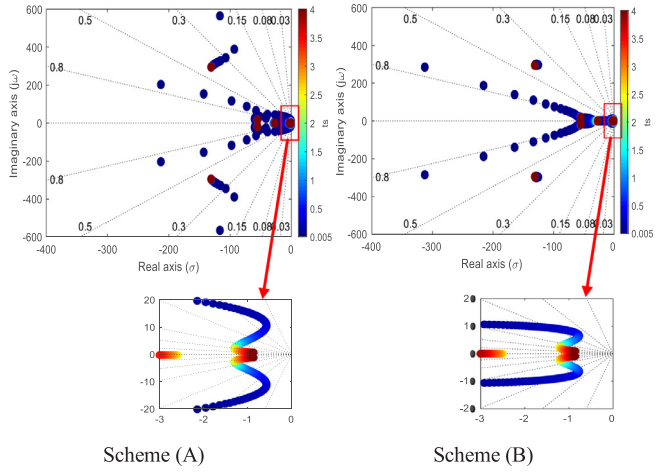

Fig. 10. System pole trajectory with respect to the PLL response time for schemes A and B.

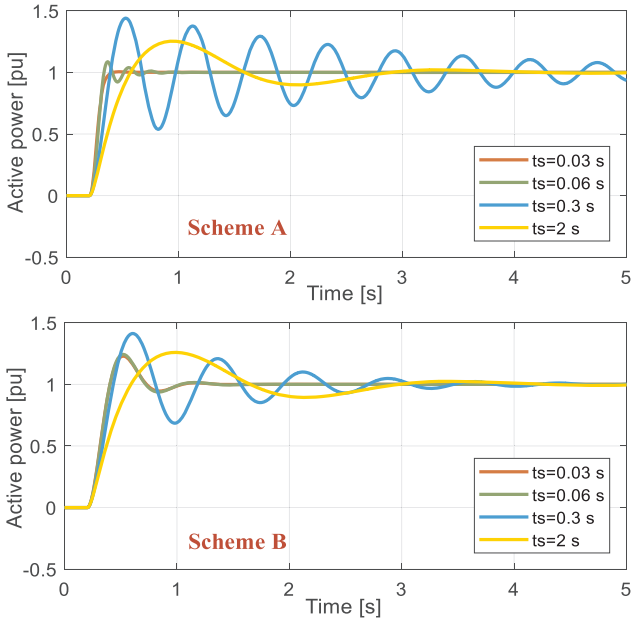

Fig. 11. Active power response with respect to the PLL response time.

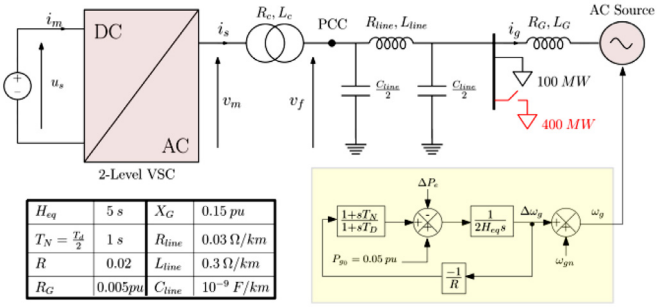

H_{eq}	5 s	X_G	0.15 pu
$T_N = \frac{T_d}{2}$	1 s	R_{line}	0.03 Ω/km
R	0.02	L_{line}	0.3 Ω/km
R_G	0.005pu	C_{line}	10^{-9} F/km

Fig. 12. Scheme of the converter that is connected to a variable frequency grid.

system for schemes A and B with respect to the PLL response time. It can be clearly seen that for a wide range of PLL response time the system stays stable.

The other result of this study is that the tuning of the PLL plays a significant role in the system response. For the given system parameters, if the PLL is fast (e.g. $t_s < 50$ ms) the dominant dynamics are mainly linked to the states in the active power control loop [17]. For the medium values of PLL response time (e.g. $100 < t_s < 500$ ms) there is a high interaction between the states in the power control loop and the states that are mainly linked with the PLL tuning in participation to the system dominant modes. For a very slow PLL (e.g. $t_s > 1$ s, which is not a realistic range) the states that are linked with the PLL tuning have the most participation rate in the dominant poles of the system.

Time domain simulation given in Fig. 11 also shows that for the fast PLL, since the dominant poles are not linked with the PLL tuning, the scheme A and B have different active power response, as expected. However, for the high value of t_s (e.g. $t_s = 2\ s$), the poles that are mainly linked with the PLL tuning become dominant and therefore we cannot see any difference between the active power response of both control schemes. Infact the dynamic response of the schemes A and B with a very slow PLL is the same as scheme C (of course with an identical value of m_p) The presented results prove the stable operation of the proposed grid-forming control variants in case of variation in the grid SCR and PLL response time.

3.2. Connection to a variable frequency grid for frequency control analysis

In order to study the frequency control capability the grid-forming control variants, the power converter is connected to a variable frequency grid, which is depicted in Fig 12. The grid parameters are given in the figure. The line length is 20 km.

Since the schemes A and B do not inherently participate in power sharing, the droop control is implemented in an outer loop (see Fig. 3) for these schemes with a 2% droop gain. The power regulation gain is kept constant at $m_p = 0.0062$ and the PLL response time is 20 ms. It is assumed that the inertia constant of the power converter is $H = 5$ s. Therefore, according to (11), ω_c has to be equal to 16.1 rad/s for the schemes A and B. For the scheme C, since m_p is the droop gain rather than an adjustable parameter, ω_c has to be changed to 5 rad/s in order to get $H = 5$ s. This reduction in the filter cut-off frequency results in power oscillations. A derivative action on the measured active power has to be utilized to eliminate these oscillations. More details about the design of this derivative action is given in [12].

A 0.4 (pu) step is applied to the load at $t = 5$ s. Fig. 13 shows the active power response of the power converter for each control scheme. During the first millisecondes, it can be noticed that the power injected to the grid is exactly the same for the three schemes. This is due to the

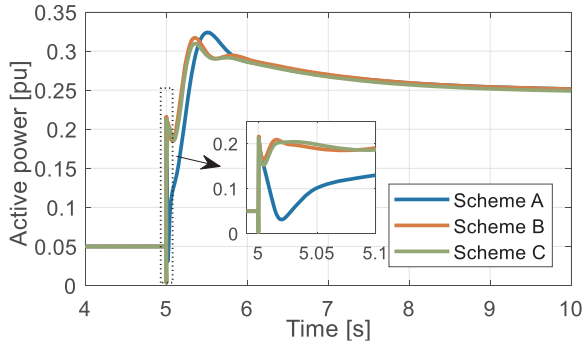

Fig. 13. Active power response of each control scheme in connection to a variable frequency grid.

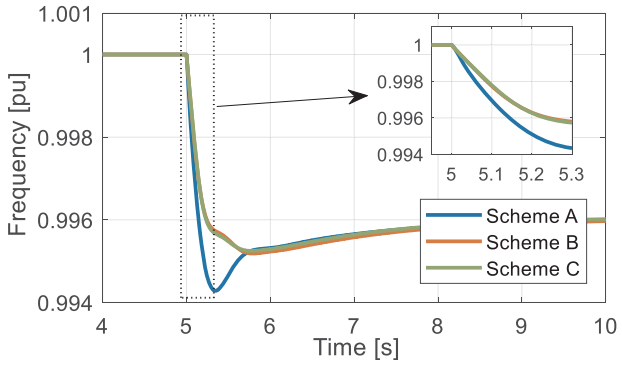

Fig. 14. Grid frequency ω_g.

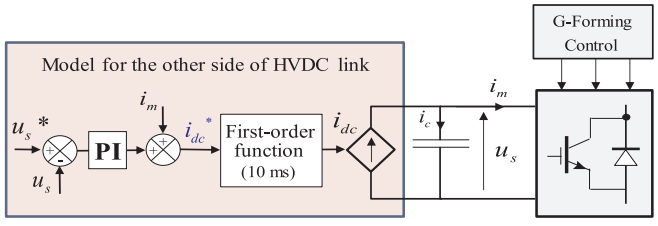

Fig. 15. Implementation of the DC bus voltage control.

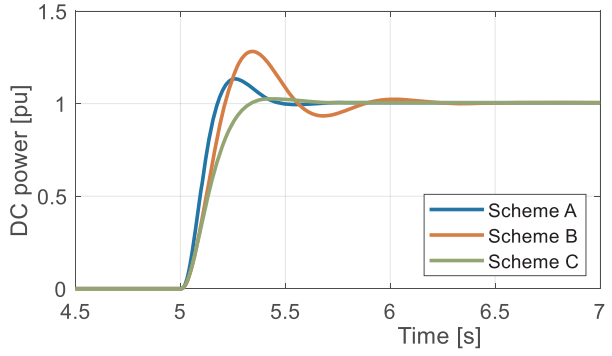

Fig. 16. Injected power from the DC bus in scenario I.

voltage source behavior of the converter. Then, the control is adjusting the angle of the modulated voltage. It can be noticed that for schemes B and C the converter injects more power after the disturbance due to the inertial effect. Fig. 14 shows the grid frequency ω_g. The improved RoCoF and frequency nadir for the schemes B and C are clearly demonstrated in this figure.

Up to here, the grid-forming control variants are introdued and their features and capabilies have been investigated with several dynamic

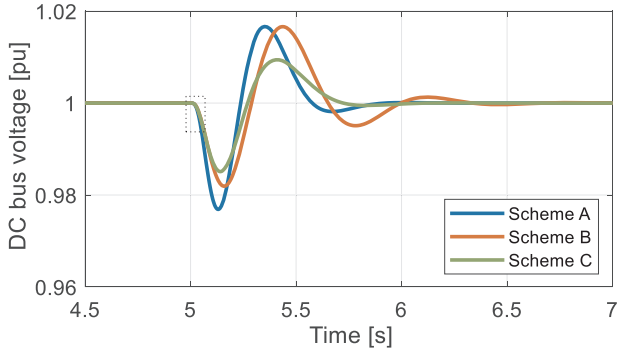

Fig. 17. DC bus voltage in scenario I.

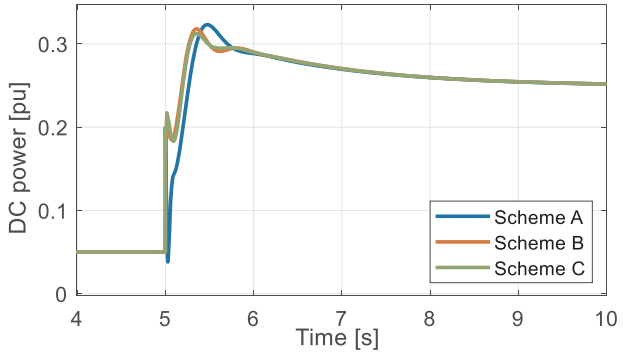

Fig. 18. Absorbed power from the DC bus in scenario II.

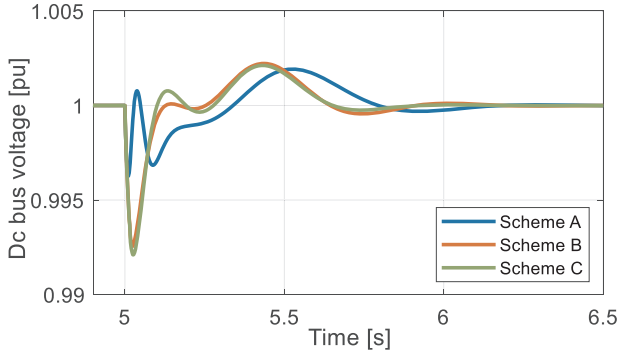

Fig. 19. DC bus voltage in scenario II.

studies. Due to the recent interest on using grid-forming controls in HDVC systems, specially for the goal of virtual inertia provision, next section is devoted to the application of the introduced control schemes in dynamic enhancement of the HVDC systems.

4. Application in HVDC systems

In this section, the effect of using grid-forming control schemes by including the DC side dynamics with application in HVDC systems is analyzed. It should be noted that only one side of the HVDC link is modeled accurately. For the other side, it is assumed that the power is assimilated to a 10 ms first order model via a controllable current source. The cable dynamics are ignored and in order to have a rough model for the DC side with realistic values, the capacitors of both HVDC substations are merged in a single capacitor, which provides a 80 ms (40 ms for each substation) inertia constant (H_{DC} = 80 *ms*) [23]. The nominal DC bus voltage is 640 kV.

Fig. 15 shows the scheme of DC side control implementation where the DC bus voltage is regulated thanks to the controlled current source. Therefore, the grid-forming converter is not performing the DC voltage

Table 2
Summary of the grid-forming control features.

Scheme	PLL	Advantages	Disadvantages
A	Yes	- Optional frequency support - Accurate power regulation -Robust against SCR variation	- No inertial effect
B	Yes	- Optional frequency support- Inertial effect	- Higher DC voltage deviation in case of frequency variation
C	No	- Inertial effect	- Higher DC voltage deviation in case of frequency variation - Compulsory frequency support

control. To design the DC voltage controller, ignoring the current source dynamics, a 300 ms response time is chosen. Two following scenarios are considered for this study.

4.1. Scenario I: step in the converter active power reference

In this scenario, the aim is to verify that the DC controller is able to regulate the DC bus voltage in such a way to keep the voltage level in the range of 5% around the nominal value. Therefore, a 1 pu step is applied to the reference power of the grid-forming converter. It is assumed that the grid frequency is fixed. The control parameters for the power converter as well as the AC grid parameters and load change scenario are the same as section III. B. A 1 pu step is applied to the reference power of the converter at $t = 5$ s. Fig. 16 shows the absorbed power from the DC bus. Fig. 17 illustrates the DC bus voltage. It can be found that the DC bus voltage is properly controlled in the acceptable range.

4.2. Scenario II: step in the load

For this case, it is assumed that the converter is connected to the variable frequency grid of Fig. 12. A step equal to 0.4 pu is applied to the AC load. Fig. 18 illustrates the absorbed power from the DC bus which is very similar to the active power at the AC side (see Fig. 12) due to the decoupling control of the DC and AC side. Fig. 19 indicates the DC bus voltage. It can be clearly seen that the DC voltage has more reduction for the schemes B and C during the first milliseconds after the disturbance. This is due to the higher demand for the energy at the AC side to provide the inertial support. Considering the obtained results for the performed studies in both AC and DC sides, Table 2 gives a summary of the features and capabilities of the proposed droop-based grid-forming control schemes.

5. Conclusions

This paper proposed a classification for the droop-based grid-forming control schemes by including a PLL on the control. Depending on the choice that is made, the service provided to the system is modified. Adding a PLL allows to get one more degree of freedom in the control and to decouple the frequency support from power control loop. Presented analysis by considering an ideal DC bus and using both system pole maps and time domain simulations proved that the proposed control schemes show different performance in case of variation of the grid SCR as well as PLL response time, while the system remains stable. Finally, by considering the DC bus dynamics the effect of each scheme on the DC bus voltage control was investigated that could give an insight to the application of the proposed control schemes in the control of an HVDC link.

Declaration of Competing Interest

The authors declare that they have no known competing financial interests or personal relationships that could have appeared to influence the work reported in this paper.

References

[1] B. Johnson, P. Denholm, B. Kroposki, B. Hodge, Achieving a 100% renewable grid, IEEE Power Energy Mag. 15 (2017) 61–73.
[2] E. Rokrok, M. Shafie-khah, J.P.S. Catalão, Review of primary voltage and frequency control methods for inverter-based islanded microgrids with distributed generation, Renew. Sustain. Energy Rev. 82 (2018) 3225–3235.
[3] S. D'Arco, J.A. Suul, O.B. Fosso, A virtual synchronous machine implementation for distributed control of power converters in SmartGrids, Electr. Power Syst. Res. 122 (2015) 180–197.
[4] F. Palombi, L. Piegari, S. D'Arco, A.G. Endegnanew, J.A. Suul, Impact on power system frequency dynamics from an HVDC transmission system with converter stations controlled as virtual synchronous machines, 2019 IEEE Milan PowerTech, 2019, pp. 1–6.
[5] S. D'Arco, G. Guidi, J.A. Suul, Operation of a modular multilevel converter controlled as a virtual synchronous machine, 2018 International Power Electronics Conference (IPEC-Niigata 2018 -ECCE Asia), 2018, pp. 782–789.
[6] M. Guan, W. Pan, J. Zhang, Q. Hao, J. Cheng, X. Zheng, Synchronous generator emulation control strategy for voltage source converter (VSC) stations, IEEE Trans. Power Syst. 30 (Nov. (6)) (2015) 3093–3101.
[7] B. Peng, X. Yin, J. Shen, J. Wang, Application of virtual synchronization control strategy in MMC based VSC-HVDC system, 2014 IEEE PES Asia-Pacific Power and Energy Engineering Conference (APPEEC), 2014, pp. 1–6.
[8] R. Aouini, B. Marinescu, K. Ben Kilani, M. Elleuch, Stability improvement of the interconnection of weak AC zones by synchronverter-based HVDC link, Electr. Power Syst. Res. 142 (Jan.) (2017) 112–124.
[9] R. Aouini, B. Marinescu, K. Ben Kilani, M. Elleuch, Synchronverter-based emulation and control of HVDC transmission, IEEE Trans. Power Syst. 31 (Jan. (1)) (2016) 278–286.
[10] A. Tayyebi, F. Dörfler, Z. Miletic, F. Kupzog, W. Hribernik, Grid-forming converters – inevitability, control strategies and challenges in future grids application, CIRED 2018 Ljubljana Workshop on Microgrids and Local Energy Communities (2018).
[11] U. Tamrakar, D. Shrestha, M. Maharjan, B.P. Bhattarai, T.M. Hansen, R. Tonkoski, Virtual inertia: current trends and future directions, Appl. Sci. 7 (7) (2017) 1–29.
[12] T. Qoria, F. Gruson, F. Colas, G. Denis, T. Prevost, X. Guillaud, Inertia effect and load sharing capability of grid forming converters connected to a transmission grid, 15th IET International Conference on AC and DC Power Transmission (ACDC 2019), 2019, p. 79 6 pp.)-79 (6 pp..
[13] P. Zhou, X. Yuan, J. Hu, Y. Huang, Stability of DC-link voltage as affected by phase locked loop in VSC when attached to weak grid, 2014 IEEE PES General Meeting | Conference & Exposition, 2014, pp. 1–5.
[14] J.J. Grainger, W.D. Stevenson, Power System Analysis, McGraw-Hill, New York, 1994.
[15] A.T. Qoria, Q. Cossart, C. Li, and X. Guillaud, "MIGRATE project, WP3 - control and operation of a grid with 100% converter-based devices deliverable 3 . 2 ;: local control and simulation tools for large transmission systems," 2019.
[16] S. D'Arco, J.A. Suul, O.B. Fosso, Automatic tuning of cascaded controllers for power converters using eigenvalue parametric sensitivities, IEEE Trans. Ind. Appl. 51 (2) (2015) 1743–1753.
[17] E. Rokrok, T. Qoria, A. Bruyere, B. Francois, X. Guillaud, Effect of using PLL-based grid-forming control on active power dynamics under various SCR, IECON 2019 - 45th Annual Conference of the IEEE Industrial Electronics Society, 2019, pp. 4799–4804.
[18] "Requirements for Generators." [Online] (2016). Available: https://www.entsoe.eu/network_codes/rfg/. [Accessed: 20-May-2019].
[19] P.C. Krause, O. Wasynczuk, S.D. Sudhoff, S. Pekarek, Analysis of Electric Machinery and Drive Systems, IEEE press, New York, 2002.
[20] T. Qoria, C. Li, K. Oue, F. Gruson, F. Colas, X. Guillaud, Direct AC voltage control for grid-forming inverters, J. Power Electron. 20 (Jan. (1)) (2020) 198–211.
[21] IEEE Power and Energy Society, IEEE recommended practice and requirements for harmonic control in electric power systems, IEEE Stand. (2014).
[22] IEEE Power Engineering Society, *IEEE guide for planning DC links terminating at AC locations having low short-circuit capacities*. ISBN 1-55937-936-7, 1997.
[23] F. Gruson, et al., Design, implementation and testing of a modular multilevel converter, EPE J. (Eur. Power Electron. Drives J.) 27 (4) (2017) 153–166.